Mean Field Stochastic Boundary Molecular Dynamics Simulation of a Phospholipid in a Membrane†

Hans De Loof,‡,§,‖ Stephen C. Harvey,*,‡ Jere P. Segrest,§ and Richard W. Pastor⊥

Department of Biochemistry and Atherosclerosis Research Unit, University of Alabama at Birmingham, Birmingham, Alabama 35294, and Biophysics Laboratory, Center for Biologics Evaluation and Research, Food and Drug Administration, 8800 Rockville Pike, Bethesda, Maryland 20892

Received September 14, 1990; Revised Manuscript Received November 26, 1990

ABSTRACT: Computer simulations of phospholipid membranes have been carried out by using a combined approach of molecular and stochastic dynamics and a mean field based on the Marcelja model. First, the single-chain mean field simulations of Pastor et al. [(1988) *J. Chem. Phys. 89*, 1112–1127] were extended to a complete dipalmitoylphosphatidylcholine molecule; a 102-ns Langevin dynamics simulation is presented and compared with experiment. Subsequently, a hexagonally packed seven-lipid array was simulated with Langevin dynamics and a mean field at the boundary and with molecular dynamics (and no mean field) in the center. This hybrid method, *mean field stochastic boundary molecular dynamics*, reduces bias introduced by the mean field and eliminates the need for periodic boundary conditions. As a result, simulations extending to tens of nanoseconds may be carried out by using a relatively small number of molecules to model the membrane environment. Preliminary results of a 20-ns simulation are reported here. A wide range of motions, including overall reorientation with a nanosecond decay time, is observed in both simulations, and good agreement with NMR, IR, and neutron diffraction data is found.

A complete understanding of relationships between structure and function of biological molecules, including membranes, requires a description of numerous interatomic interactions. As demonstrated by the success in the modeling of proteins and nucleic acids (McCammon & Harvey, 1987; Brooks et al., 1988), molecular dynamics (MD)[1] simulations are well suited to handle such a level of complexity. Nevertheless phospholipid bilayers forming membranes, or phospholipid monolayers found in plasma lipoproteins, have only begun to receive attention (van der Ploeg & Berendsen, 1982, 1983; Northrup, 1984; Northrup & Cuvin, 1985; Egberts, 1988; Egberts & Berendsen, 1988; Edholm & Johansson, 1987; Watanabe et al., 1988; Harris & Rice, 1988; Wendoloski et al., 1989).

The paucity of membrane MD studies is due to a number of inherent difficulties caused by (i) the dynamic nature of the liquid-crystalline state, requiring the calculation of multinanosecond trajectories; (ii) the large dimensions and heterogeneous composition of membranes; (iii) and the complex, often curved or highly charged, interface, requiring a sophisticated treatment of boundary conditions and electrostatics (Gennis, 1989; Jain, 1988; Cevc & Marsh, 1987). Since MD simulations of large systems, such as the periodic boundary membrane models (Egberts & Berendsen, 1988), are restricted to several hundred picoseconds even on a supercomputer, progress has been understandably slow. In addition, because the biologically active membrane exists above the gel to liquid crystal phase transition (Gennis, 1989), structural methods such as X-ray and neutron diffraction do not provide atomic resolution data or adequate starting structures for the molecular dynamics simulations.

The difficulties associated with MD of bilayers prompted us to pursue the simulation strategy outlined in Figure 1. The first step, described by Pastor et al. (1988a), consisted of a 200-ns Brownian (or diffusive) dynamics simulation of a single chain. The effect of the surrounding bilayer on the equilibrium properties was parameterized by an averaged interaction determined by the strength of a Marcelja-type mean field (Marcelja, 1973; Schindler & Seelig, 1975; Pastor et al., 1988a). The dynamical or collisional effects of the surrounding medium were simulated by replacing deterministic equations (classical MD) with stochastic equations; in Brownian dynamics (BD) the trajectory is modulated by random displacements whose magnitudes are related to the effective viscosity of the solvent. Because the first three atoms of the chain were anchored, overall rotation was neglected; i.e., only internal motions such as gauche–trans isomerization and torsional libration were explicitly simulated. The effects of axial rotation and wobble were then calculated analytically (Pastor et al., 1988b), assuming uncoupling of internal and overall motion; it was, in fact, necessary to include these additional degrees of freedom to obtain a good fit between simulation and experiment.

This paper presents the second and third steps shown in Figure 1. First, the simulation of a single chain is extended to a complete DPPC molecule, with two important modifications: (i) the lipid is only anchored at the phosphorous atom, thereby allowing overall rotational degrees of freedom; (ii) the trajectory is generated by Langevin dynamics (LD) (rather than BD), so that inertial terms are included. The second part of this paper introduces a hybrid simulation method, *mean*

† This work was supported by grants from the National Institutes of Health (GM-34015 and HL-34343) and from the National Science Foundation (DMB-87-06551). H.D.L. was partially supported by a NATO Postdoctoral Fellowship.

* Address all correspondence to this author.

‡ Department of Biochemistry, University of Alabama at Birmingham.

§ Atherosclerosis Research Unit, University of Alabama at Birmingham.

‖ Present address: Department of Medical Biophysics, Karolinska Institutet, Box 60400, S10-401 Stockholm, Sweden.

⊥ Food and Drug Administration.

[1] Abbreviations: MD, molecular dynamics; DPPC, dipalmitoylphosphatidylcholine; LD, Langevin dynamics; BD, Brownian dynamics.

0006-2960/91/0430-2099$02.50/0

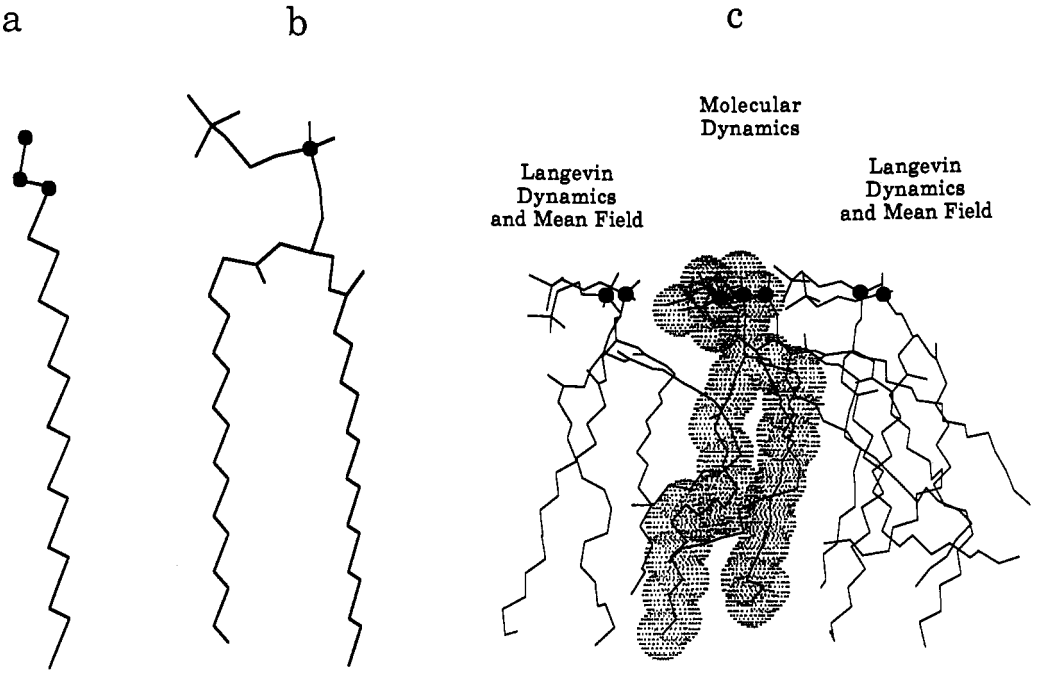

FIGURE 1: Strategy used in the present study for the stochastic simulation of a membrane. The filled circles indicate which atoms are anchored to the laboratory frame. (a) The single-chain model previously described by Pastor et al. (1988a,b, 1990a,b). (b) Single-molecule simulations of a complete DPPC molecule. The standard IUPAC nomenclature is used; the *sn*-1 chain is on the right; the *sn*-2 chain is on the left. Within each chain, carbons are numbered sequentially; C1 is the carbonyl carbon and C16 is the last carbon in the chain. (c) Hexagonally packed monolayer containing seven molecules. In the latter system conventional MD is used on those molecules that are surrounded by other explicitly treated molecules; molecules in the boundary layer are treated by Langevin dynamics plus a mean field, to mimic volume exclusion and collision effects from molecules beyond the boundary layer.

field stochastic boundary dynamics, and reports our preliminary results on a hexagonal array of seven lipids. As shown schematically in Figure 1c, the mean field potential is applied only to a boundary layer of lipids, which is simulated by using Langevin dynamics; the center of the system (reaction region) is simulated by using classical molecular dynamics with no explicit mean field. The method is designed to address the deficiencies of both the single-chain mean field simulations and periodic boundary MD: the bias introduced by the mean field is reduced, while the number of explicit atoms in the system is still small enough to permit multinanosecond simulations. This approach is based on the stochastic boundary dynamics technique already applied to proteins (Berkowitz & McCammon, 1982; Brooks et al., 1985) but differs in that a mean field tailored to liquid crystal systems is utilized.

During these different steps, the objective remains to obtain close agreement between the properties of the simulated system and the experimentally determined values and to maintain self-consistency of the boundary and reaction region. This is primarily done by tuning the strength of the mean field components. The most important experimental data to compare with are the observations made by NMR techniques: the deuterium NMR order parameters determined by Seelig et al. (1974, 1980) and the T_1 spin–lattice relaxation times, determined at different field strengths, by Brown and coworkers (1983). In addition, we compare the simulated dimensions with those obtained by neutron diffraction techniques (Zaccai et al., 1979) and the fraction of gauche isomers with IR spectroscopic observations (Mendelsohn et al., 1989).

METHODS

Dynamics Algorithm. While molecular dynamics simulations of single molecules in vacuo often yield useful results for proteins and nucleic acids, neighboring acyl chains significantly affect the dynamics of a lipid in a membrane. The explicit incorporation of these molecules is one possible solution. An alternative approach is to estimate the average dynamic effect of neighboring molecules on the basis of an estimate of the viscosity, by using a stochastic algorithm for generating the trajectories (McCammon & Harvey, 1987). The accuracy of the different algorithms for the propagation of atomic coordinates has recently been investigated, allowing an informed choice at a given viscosity and timestep (Pastor et al., 1988c).

The Langevin algorithm used here was originally described by Brunger et al. (1984):

$$x_{n+1} = x_n + (x_n - x_{n-1})\frac{(1 - (1/2)\gamma\Delta)}{(1 + (1/2)\gamma\Delta)} + \frac{(\Delta^2/m)(F_n + R_n)}{(1 + (1/2)\gamma\Delta)} \quad (1)$$

where x_{n-1}, x_n, and x_{n+1} are the coordinate positions at successive timesteps, γ is the collision frequency, Δ is the timestep, F_n and R_n are the systematic and random forces applied at step n, and m is the mass of the particle. This random force, which mimics the collisions with the surrounding molecules not explicitly treated in the system, is taken from a Gaussian distribution of mean zero and variance $2m\gamma kT/\Delta$, where k is Boltzmann's constant and T is the absolute temperature. When the collision frequency is zero, this algorithm is equivalent to the Verlet molecular dynamics algorithm (Verlet, 1967; McCammon & Harvey, 1987).

The timestep used in all simulations was 2 fs. The collision frequency of all atoms in the one molecule simulation was set at 50 ps^{-1}. This value yielded a good fit with the NMR data of Brown et al. (1983) in the Brownian dynamics simulations of Pastor et al. (1988b).

All calculations were carried out at a temperature of 324 K (51 °C), well above the phase transition temperature of DPPC (41.5 °C), as we are primarily interested in the characteristics of the liquid-crystalline membrane.

Mean Field Model. The anisotropic lipid environment of the phospholipid molecule is modeled by using a mean field,

adapted from the single-chain simulations of Pastor et al. (1988a), which in turn was based on the mean field theory of Marcelja et al. (1973, 1974). The mean field consists of two components, a repulsive term and a dispersive term. This mean field theory, as applied by Schindler and Seelig (1975), Gruen (1985), and Pastor et al. (1988a, 1990a,b), accurately models a number of equilibrium properties of DPPC bilayers such as the deuterium NMR order parameters. It is, however, our goal to reduce the effect and/or bias on the dynamics of the DPPC molecule induced by the parametrization of the mean field by ultimately applying it only on the boundary of the system.

The repulsive or steric potential is related to the surface pressure and acts on the last carbon of the lipid chain. It is inversely proportional to the distance between the terminal carbon atom and a surface, located at z_0, that is parallel to the bilayer interface. In our coordinate system the xy plane is located in the headgroup region of the molecule and the chains are extended in the $-z$ direction. The repulsive potential is thus

$$E_{rep} = \sum_{chains} \frac{\Gamma}{(z_{16} - z_0)} \quad (2)$$

where z_{16} is the z coordinate of the last carbon in the chain, z_0 is the z coordinate of a reference plane parallel to the interface, and Γ is the field strength.

The second term, the dispersive potential, is proportional to the molecular order parameter. This term simulates the van der Waals interactions with the surrounding lipid molecules and is a Maier-Saupe (1959) type potential:

$$E_{disp} = \sum_{\substack{chain \\ carbons}} -\Phi(1/2)(3\cos^2\beta_i - 1) \quad (3)$$

$(1/2)(3\cos^2\beta_i - 1)$ is the order parameter of the chain, where β_i is the angle between the bilayer normal and the long axis of the molecule (the vector normal to the plane spanned by the two C–H vectors) and Φ is the field strength. The Marcelja (1973, 1974) dispersive term also included a term proportional to the fraction of dihedral angles in the trans state. In contrast to the work of Pastor et al. (1988a), this term was not included here, because of computational efficiency. The strength of each component of the mean field is parameterized in order to reproduce the experimental deuterium NMR order profile (Seelig & Seelig, 1980).

Since no water molecules are treated explicitly, an additional constraint is needed to prevent the carbon atoms C2–C16 of both chains from moving into the aqueous phase. The exact location of the plane defining the lipid–water interface (z_0) was subject to investigations. This surface always coincided with the surface used to calculate the repulsive mean field component:

$$E_{sur} = \sum_{\substack{chain \\ carbons}} k_{dist}(z - z_0)^2 \quad \text{if} \quad z \geq z_0$$

$$E_{sur} = \sum_{\substack{chain \\ carbons}} 0 \quad \text{if} \quad z < z_0 \quad (4)$$

where the force constant k_{dist} = 1.0 kcal/mol Å^2. In order to avoid a divergence in the repulsive energy, z_0 was set 1 Å smaller for the terminal carbon atoms (during the simulations the C16, however, rarely approaches the surface).

The phosphorous atom was fixed to the origin of the coordinate system with a harmonic constraint (k = 100 kcal/mol Å^2) and the N atom of the headgroup was constrained to the xy plane (z = 0) with a force constant k = 5 kcal/mol Å^2. This is important for the simulations with several molecules, where the constraint helps to simulate the surface area occupied by the molecule (see below). All parameters were varied, on a trial and error basis, to obtain average molecular properties compatible with experimental values.

Molecular Mechanics Parameters. The potential function included harmonic bond and angle terms, and improper torsions to preserve chirality of the glycerol carbon 2 and planarity of the carbonyl bond. Standard dihedral potentials were used except for the alkane chains where the popular Ryckaert-Bellemans (1975) potential, a power series in cos Φ, was used. Nonbonded interactions included only a 6-12 Lennard-Jones potential (cutoff 8 Å). The nonbonded list was updated every 25 steps. As our major interest was focused on the hydrocarbon region, no electrostatic terms were included. Most of the molecular mechanics parameters were taken from the AMBER force field (Weiner et al., 1984) and missing parameters were taken from Egberts et al. (1988). A complete description of the energy function and the parameters is contained under Appendix.

Starting Structures, Monolayer Assembly. The starting structure of the single DPPC molecule was modeled after the crystal structure of dilauroylphosphatidylethanolamine (Elder et al., 1977) by using the SYBYL (TRIPOS) software and was equilibrated for 300 ps. For the hexagonal phospholipid monolayer system, the starting structure is more critical and was obtained as follows: seven conformations, chosen at random from the one molecule simulation, were assembled by assuming a hexagonal packing and a surface area of 68.9 Å per molecule (Pastor et al., 1990b). Phosphorous and nitrogen atoms were constrained to the xy plane, while the hydrocarbon tails extended into the $-z$ direction. This assembly was then subjected to minimization (simplex minimization and steepest descent) to remove bad contacts resulting from the assembly procedure. The procedure did not induce dramatic changes in the overall structure (Venable and Pastor, manuscript in preparation). The system was equilibrated for a period of 1 ns.

In the seven molecule simulations the constraints on the headgroups of the boundary molecules are somewhat different. The phosphorous atom of the central molecule was fixed as in the one-molecule simulation but those in the boundary are constrained on the xy plane [k = 100 kcal/(mol Å^2)]. In addition, pseudobonds between all neighboring phosphorous atoms keep the molecules together and impose an average surface area per molecule on the system. The force constant for these pseudobonds was k = 20 kcal/(mol Å^2).

Stochastic Boundary. An essential feature of the stochastic boundary methods is a partitioning of the many-body system into several regions (Berkowitz & McCammon, 1982; Brooks et al., 1985). A central region or reaction region, the site of major interest, is simulated by classical molecular dynamics. It is surrounded by a bath or boundary region that should simulate the true surroundings of the reaction region in at least two ways: preserve the equilibrium structure and structural fluctuations of the reaction region and allow the appropriate energy fluctuations to occur between them. It should thus contribute to the longer range nonbonded interactions of the reaction region. The use of the Langevin algorithm gives this region its temperature bath properties.

In simulations of liquids, where the relative position of the molecules is not fixed, a third region called a reservoir region is required. This reservoir region is needed to contain the system and to stimulate the movement of atoms in and out of the bath and reaction compartment (Berkowitz & McCammon, 1982). In proteins, where the atomic positions

are relatively fixed, such a region can be omitted by introducing constraints or a mean field, on the atoms in the boundary (Brooks et al., 1985). We adopt this second variant, thereby ignoring lateral diffusion. In phospholipid membranes lateral diffusion is on average less than 0.1 Å/ns (Gennis, 1989) and for the timescales involved in this work the error is thus small.

We investigated two ways of partitioning the system. In the first, the mean field and LD were applied to the boundary layer of lipids, and MD was applied to the central lipid, regardless of the precise orientation of the chains. The collision frequency was set to 25 ps^{-1} on the boundary lipids; this reduction of 50% compared to the previous single-chain simulations was based on the notion that, on average, only half of the molecule was surrounded by real atoms.

In a second series the reaction region consisted of a cylindrical region with an 8-Å diameter, centrally located around the z axis. The boundary atoms (i.e., all atoms outside this central cylinder) were treated with Langevin dynamics; their collision frequency was gradually increased from zero to 50 ps^{-1} between a distance of 4 and 8 Å from the central z axis with the use of a switching function. A similar switching function was imposed in the headgroup region, from 50 ps^{-1} LD at the xy plane, where the phosphorous atoms were constrained, to classical MD at the "interface", a plane with z = −4 Å. (When both conditions occurred the larger collision frequency was chosen.) The values of the collision frequencies were updated simultaneously with the nonbonded list, every 25 steps.

Dihedral Transition Rates. Transitions over the barriers between the trans and gauche conformations were monitored during the simulations. A transition was counted when the dihedral angle crossed the barrier and reached the bottom of the well of the new conformation. Rate constants were calculated by dividing the number of transitions out of a particular state by the time spent in that state. This procedure, also called "simple counting", may overestimate the number of transitions when solvent damping is ineffective or when recoil into the reactant well is a frequent event (Pastor & Karplus, 1989). To validate the simple counting procedure we performed a Hazard analysis (Helfand, 1978); i.e., we analyzed the first passage times (time needed for the first arrival at the next minimum) and checked if this was compatible with a simple Poisson process. At the collision frequencies used in these simulations the Hazard plots were quite linear (data not shown), indicating that there was not a larger-than-expected number of short first passage times or the presence of recoil. We observed the presence of recoil only when the collision frequency was set at 5 ps^{-1} or lower, and this phenomenon affected mainly the dihedrals with the faster transition rates (i.e., those at the end of the chains).

Deuterium NMR Order Parameters. The deuterium order parameter S_{CD} is a critical source of structural information for lipid bilayers (Seelig & Seelig, 1980). It is related to the average orientation of the methylene group:

$$S_{CD} = \tfrac{1}{2}\langle 3\cos^2\theta - 1\rangle \quad (5)$$

where θ is the angle between the vector along the carbon–deuterium bond and the bilayer normal. This parameter varies between −0.5, for a fully extended all-trans chain, and 0 for a completely random orientation of the chain. This property was calculated every 10 steps during the simulations.

NMR Spin–Lattice Relaxation Times. The most complete frequency-dependent ^{13}C T_1 relaxation measurements of the methylene groups in DPPC single bilayer vesicles were made by Brown and co-workers (1983). Their data were obtained at seven different spectrometer frequencies (15, 20, 25.1, 45.3, 75.5, 90.5, 126 MHz carbon). The relationship between these measurements and the motions of the molecule can be determined from the following correlation function (Lipari & Szabo, 1982):

$$C(t) = \tfrac{2}{5}\langle P_2[\mu(t)\cdot\mu(0)]\rangle \quad (6)$$

where P_2 is the second Legendre polynomial and μ is a unit vector pointing along a C–H bond in the laboratory frame, when vesicle rotation, a process evolving at the microsecond timescale, can safely be ignored. The ^{13}C spin–lattice relaxation is given by the following equation (Lipari & Szabo, 1982):

$$1/NT_1 = (\hbar\gamma_C\gamma_H/r^3)(1/10) \times [J(\omega_C - \omega_H) + 3J(\omega_C) + 6J(\omega_C + \omega_H)] \quad (7)$$

where N is the number of hydrogens bonded to the carbon, $\hbar$ is Plank's constant divided by 2π, r is the C–H bond distance (1.1 Å), γ_C, γ_H, and ω_C, ω_H are the gyromagnetic ratios and Larmor frequencies of the ^{13}C and ^1H nuclei, and $J(\omega)$ is the spectral density of the $C(t)$ correlation function described above. The spectral densities were determined indirectly after curve fitting the correlation decays with up to four exponentials. The parameters for these fits were obtained by using a grid search followed by a Levenberg-Marquardt method (Press et al., 1988). For these calculations we used the first 5000 points (5 ns) of the correlation functions. To facilitate the curve fitting, the plateau value, obtained directly from the trajectory, was subtracted from the correlation function in the following way:

$$\frac{C(t) - C(\infty)}{C(0) - C(\infty)} \quad (8)$$

It is convenient to use the formulas 18a–c in Pastor et al. (1988b) as they ensure positive values for all coefficients.

Coordinate Statistics, Correlation Functions. Coordinates were saved every picosecond. Autocorrelations were calculated with the use of fast Fourier-transform routines (Press et al., 1988). The P_2 correlation functions were obtained from the trajectories by using the $l = 2$ spherical harmonic correlation functions [see also Pastor et al. (1988b)]. This enables the use of a fast-Fourier-transform routine and has the added advantage of giving information about rotational averaging.

Computer Resources. All programs were written in the C language and were based on the *yammp* package developed by R. Tan (Tan & Harvey, 1989). Calculations were performed on Silicon Graphics 4D/25, 4D/220GTX, and 4D/240GTX workstations and on several Vaxstations. A small number of calculations were performed on a Cray XMP/24. One nanosecond of simulation of one DPPC molecule took about 44 h on a Microvax II. On the Silicon Graphics 4D/220 workstation, using one processor, the time required was 2 h. One nanosecond of simulation of the seven-molecule monolayer system took about 23.6 h on the latter machine or 7.6 h on the Cray XMP/24.

Results

Single-Molecule Simulations. In comparison to the single-chain simulations performed by Pastor et al. (1988a), our DPPC molecule has additional degrees of freedom, since it is only anchored at one atom, the phosphorous atom, instead of the first three atoms in the chain. As a result overall rotations are allowed and it might be expected that a relatively stronger mean field would be needed. There are, however, two chains present, which reduces the need for a stronger mean field, as more of the surroundings are occupied by real atoms. There

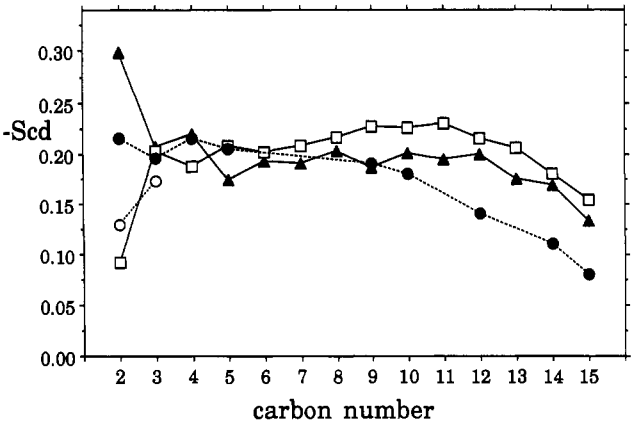

FIGURE 2: Deuterium NMR order parameters for the 102-ns single molecule simulation, together with the experimental data of Seelig and Seelig (1974, 1980). Experimental values are connected with a dotted line for the *sn*-1 chain (filled circles) and the values for C2 and C3 on the *sn*-2 chain (open circles). Simulation data are the averages over both hydrogens on each carbon and are shown for the *sn*-1 chain (triangles) and the *sn*-2 chain (squares).

is probably not one set of parameters for the mean field that would yield the best fit with experimental observations, but, instead, several combinations of parameters are likely to yield good results. As the computer time needed for equilibration is quite extensive, we did not attempt to span the parameter space exhaustively. A relatively good fit with the experimental deuterium order parameters was obtained with $\Gamma = -10.5$ (kcal Å)/mol and $\Phi = 0.21$ kcal/mol. These values are similar to those used by Pastor et al. (1988a, 1990b) in the one-chain simulations, and it seems therefore that the opposing tendencies described above cancel each other. The repulsive "surface" was located at −4 Å, close to the carbonyl bonds of the molecule. Below we describe the results of a 102-ns simulation.

Figure 2 shows the deuterium NMR order parameter profile of this simulation, together with the experimental values determined by Seelig (1980). A number of aspects are clearly in agreement with experiment: a plateau is present in the middle of the chain, between carbons 3 and 11, whereafter the order parameter drops, reflecting increased disorder in the center of the membrane. The order parameters of the carbons on both chains are very similar, except at the branching of the chains. The individual order parameters of the two hydrogens on each carbon are nearly identical, indicative of rotational symmetry: the average absolute difference between them, for all carbons on the *sn*-1 chain, was 0.0107. An important exception to these last two observations occurs at the origin of the *sn*-2 chain, in agreement with experiment. This is because of a kink in the *sn*-2 chain, necessary for the parallel alignment of both hydrocarbon chains in the membrane. The average for both hydrogens of C2 on *sn*-2 is close to the experimental average (0.092 versus 0.12), but the difference between them was somewhat too large (0.26 versus 0.053). We note that the order parameters of C2 on both chains were the slowest to converge and show the largest differences with the experimental values. This is most probably due to the simple nature of the repulsive surface modeling the interface.

Figure 3 shows graphically the type of motions occurring at different time scales: in each part of the figure ten consecutive coordinate sets are superimposed with time intervals between frames changing by a factor of 10, from 100 fs to 10 ns.

It is clear that the conformational space of the DPPC molecule within this mean field is very large, and it is therefore expected that relatively long simulations are needed in order to reach equilibrium. This is illustrated in Figure 4a where

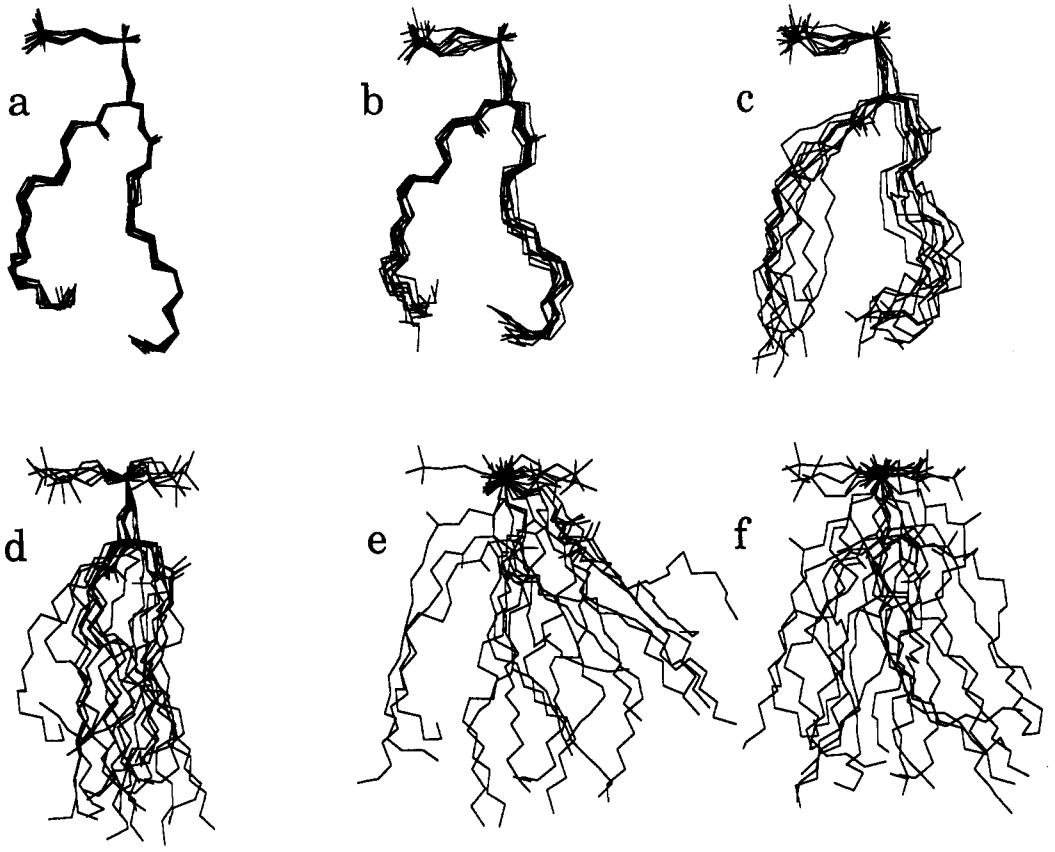

FIGURE 3: Superposition of 10 consecutive time frames of the single-molecule simulation. The time interval between superimposed coordinate sets varies from 100 fs (a) to 10 ns (f), increasing by a factor of 10 between each part of the figure.

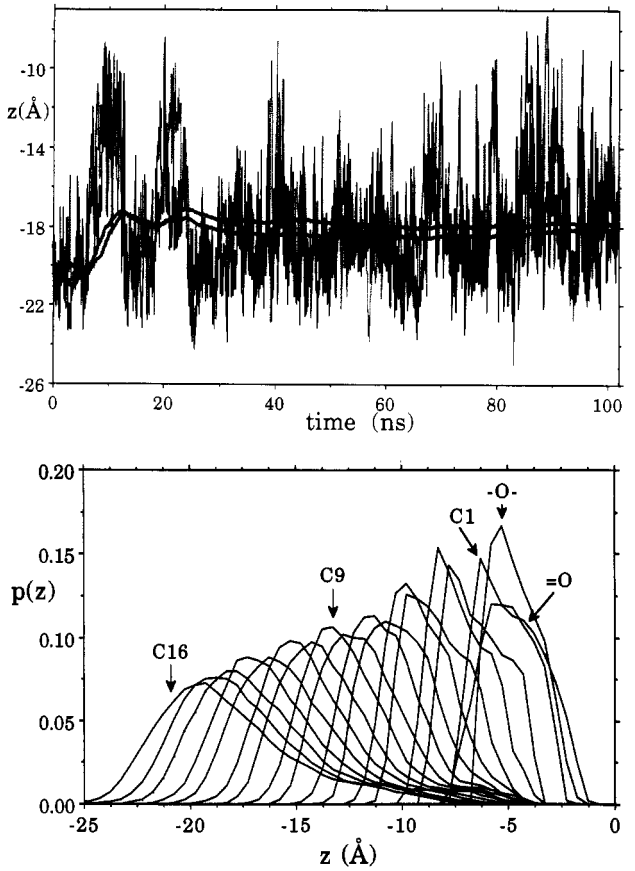

FIGURE 4: (a, Top) Cumulative average (thick lines) of the z coordinate of the terminal carbon atoms (C16) of both chains. The upper line is for C16 of the *sn*-2 chain. Also shown are the averages over 60-ps intervals (dotted line, *sn*-2 chain). Note the large amplitude of the motions and the time needed for the cumulative average to reach equilibrium. (b, Bottom) Probability distribution, in 0.5-Å intervals, for the z coordinates of the carbon and oxygen atoms of the *sn*-1 chain. Although there is explicit repulsion from a surface located at −4 Å (E_{sur}) for the carbons C2–C16, it is not perturbing the distribution of the atoms at the chain origin. When this surface was placed at −2 Å, however, distorted or bimodal distributions were produced (data not shown).

the evolution of the z-coordinate position is plotted for the two terminal carbon atoms, together with a cumulative average of these values. Note the large amplitude of the fluctuations of the z coordinate. The average distance, along the bilayer normal, between the phosphorous atom and C16 was 18.13 and 17.84 Å for the *sn*-1 and *sn*-2 chains, respectively. If we assume a distance of 2 Å between the terminal carbon atoms of opposing monolayers, a P–P distance of 38 Å is obtained, as compared to a value of about 40 Å obtained by Lewis and Engleman (1983). The C4–C4 distance of 24.2 Å obtained by Zaccai et al. (1979) compares to a value of 25.13 Å in our simulation. The average dimension of the molecule is accurate within the errors of the experimental observations. Also of interest is the nearly equal length of both chains.

Figure 4b shows the probability distribution function for the z coordinates of the carbon and oxygen atoms of the *sn*-1 chain. There is little noise in these distributions, indicating that the conformational space has been adequately sampled during the simulation. The surface constraint, prohibiting C2–C16 from crossing the interface and mimicking the presence of the aqueous phase, was located at −4 Å. Other locations (e.g., −2 Å) resulted in distorted or bimodal distributions of several carbon atoms near the headgroup (data not shown). As it is generally believed that water penetrates the membrane up to the carbonyl region, or about −4 Å from the

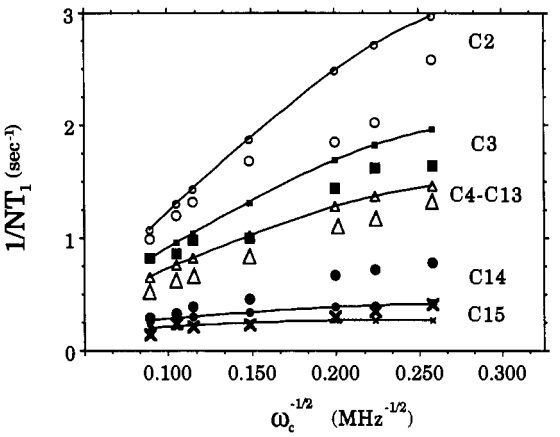

FIGURE 5: $1/NT_1$ versus $\omega_C^{-1/2}$ for the 102-ns single-molecule simulation compared with the experimental values obtained by Brown et al. (1983). Data from the simulations are connected with a line and have the smaller symbols: C2 (open circles), C3 (squares), C4-C13 (triangles), C14 (filled circles), and C15 (x).

phosphorous atom, this surface mimics this effect in a simple but apparently adequate way.

From the results in Figure 3 as well as from the large-amplitude motions of the terminal carbon atoms shown in Figure 4a, it is clear that nanosecond time scale motions are present in our simulations. It is therefore interesting to compare our simulations with the NMR spin–lattice relaxation times determined by Brown et al. (1983). Within the range of field strengths used in those experiments (15–126 MHz), only the presence of motions on the nanosecond time scale would result in frequency dependence of the observed values, while motions outside this range only contribute to their magnitude. Obtaining these values from the trajectories involved the calculation of the reorientational relaxation of the carbon–hydrogen bond vectors in the laboratory frame. The resulting correlation function was fitted with up to four exponential functions. Three exponentials were always needed, and clearly demonstrated the presence of a nanosecond time scale component. (See Table I for more information about these curve fits.) Using a fourth exponential resulted, not unexpectedly, in slightly improved fits, primarily for the short-time decay, but this did not have a major effect on the calculated T_1 relaxation times. Figure 5 compares the experimental results with those from the simulation. As only one experimental value is available for carbons 4–13, we have averaged the values obtained from the simulations. The overall agreement with experiment was good, although the frequency dependence for C14 and C15 is somewhat too small. This may be an artifact of the repulsive mean field component acting on the terminal carbon atom. (This possibly also explains why the order parameters at the end of the chain do not drop as low as the experimental values in Figure 2.)

In the single-chain simulations of Pastor et al. (1988b), it was necessary to superimpose analytically a slow component (axial rotation and wobble) to the dynamics obtained from the simulation in order to obtain a good fit with the experimental data. In the present simulation there is agreement with experiment without any additional model-dependent assumption; i.e., the motions present in the trajectories account for nearly all the frequency dependence observed experimentally. The overall agreement with experiments validates our choice of the collision frequency, the strength of the mean field components, and the way our molecule is constrained at the interface. This allows us to further analyze the motions occurring in the model system, properties that are difficult or impossible to probe

Table I: Curve Fitting for Calculation of T_1[a]

carbon	H	τ_1	τ_2	τ_3	a_1	a_2	a_3	$\sum_{i=1}^{3}(a_i\tau_i)/\sum a_i$	$\sum_{i=1}^{4}(a_i\tau_i)/\sum a_i$
2	1	5.058	69.06	1426.9	0.5283	0.3677	0.1040	176.5	173.7
	2	3.339	64.12	1236.2	0.4482	0.4387	0.1131	169.5	170.5
3	1	2.121	45.27	1159.1	0.4703	0.4556	0.0741	107.5	107.9
	2	2.850	58.00	1181.4	0.5209	0.4062	0.0729	111.2	111.6
4	1	2.115	44.25	954.7	0.4346	0.4809	0.0845	102.9	103.9
	2	2.948	48.63	1328.7	0.4793	0.4428	0.0779	126.5	127.0
5	1	3.977	59.04	917.4	0.5471	0.3831	0.0697	88.8	87.5
	2	4.033	61.64	1361.9	0.5545	0.3748	0.0707	121.6	124.6
6	1	3.847	58.07	1238.4	0.5519	0.3796	0.0684	108.9	84.9
	2	3.847	58.07	1238.4	0.5519	0.3796	0.0684	108.9	110.2
7	1	3.361	47.85	860.1	0.5287	0.3973	0.0740	84.4	85.3
	2	2.777	44.05	1202.0	0.4916	0.4379	0.0704	105.3	104.9
8	1	4.721	57.35	871.5	0.6112	0.3252	0.0636	77.0	74.6
	2	3.784	53.20	1393.4	0.5685	0.3692	0.0622	108.5	115.3
9	1	4.626	53.58	863.6	0.6226	0.3246	0.0528	65.9	65.4
	2	4.790	58.13	1577.5	0.6321	0.3178	0.0502	100.6	108.3
10	1	3.440	44.44	962.3	0.5846	0.3676	0.0478	64.4	66.1
	2	4.057	49.04	1387.1	0.6218	0.3305	0.0477	84.9	91.8
11	1	3.262	38.89	856.3	0.6021	0.3486	0.0493	57.7	58.6
	2	3.719	47.09	1151.1	0.6348	0.3245	0.0407	64.4	68.0
12	1	3.157	35.52	858.4	0.6397	0.3269	0.0334	42.3	42.6
	2	2.874	41.84	1228.5	0.6189	0.3561	0.0250	47.3	47.3
13	1	2.438	32.65	966.3	0.6208	0.3591	0.0201	32.7	32.0
	2	2.457	35.77	1098.6	0.6254	0.3563	0.0183	34.4	34.4
14	1	2.635	30.68	1065.3	0.7250	0.2616	0.0134	24.2	23.7
	2	2.564	31.04	758.9	0.7121	0.2764	0.0115	19.1	19.4
15	1	2.121	17.87	490.9	0.7128	0.2714	0.0159	14.1	12.1
	2	2.246	24.15	623.6	0.7501	0.2404	0.0095	13.4	12.4

[a] Coefficients and amplitudes for the three-exponential fits of the P_2 correlation function for both carbon–hydrogen vectors of the *sn*-1 chain. Time is in picoseconds. The last two columns summarize the results by showing the overall relaxation time of the three-exponential fit together with the end result for the four-exponential fit. Fits were based on the first 5000 points of the correlation function (5 ns).

experimentally in a direct way.

A useful marker of the dynamic behavior of this system is the dihedral transition rate. Figure 6 shows these values for the dihedrals in the alkane chains that are represented by the Ryckaert Bellemans potential (from the dihedral around the C3–C4 bond, up to the end of the chain). A total of 27 864 transitions were observed for these dihedrals during the 102-ns simulation. As previously observed by Helfand (1984) and Pastor et al. (1988a), once a dihedral is more than three atoms from the end of a chain, the isomerization rate becomes constant, because annealing around the new conformation is the principal isomerization mechanism, rather than swinging of the complete chain around that particular bond. We observe that both chains have similar characteristics, except for the beginning of the chains where the kink in *sn*-2 significantly reduces the total number of transitions. Further details on the number of transitions are given in Table II. It is interesting to note that during the complete simulation one g^- to g^+ transition occurred for the last dihedral of the *sn*-2 chain, in spite of the high barrier (~10 kcal/mol). From the difference with the g–t barrier (~3 kcal/mol) one such transition is expected for about every 5000 t to g^- transitions, and we observed 6804 of those during the complete simulation.

The average gauche fraction of all these dihedrals is 0.245, close to the value of 0.24 recently determined by Mendelsohn et al. (1989) using infrared spectroscopy. This corresponds to 3.6 gauche bonds per chain. The mean field, or the organization of the molecule in a membrane environment, thus significantly reduces the fraction of bonds in the gauche conformation as compared to a value of 0.336 that would be expected from the Ryckaert Bellemans potential without van der Waals interaction. In parallel with the order parameters, the fraction of gauche bonds in the middle of the chain is nearly constant, with a slight increase toward the end of the chain, as was also observed in the experiments of Mendelsohn et al. (1989).

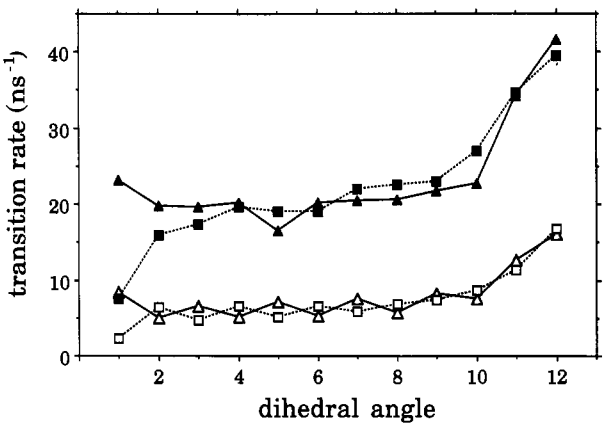

FIGURE 6: Transition rates of the dihedral angles of both chains estimated by using the "simple counting" procedure. All dihedrals have the Ryckaert-Bellemans (1975) torsional potential; the first dihedral corresponds to the one between C3 and C4 (for additional details on these dihedrals, see Table II). Trans–gauche rates are in the lower part of the figure (open symbols) and gauche–trans rates are in the upper part (filled symbols), for the *sn*-1 chain (triangles) and the *sn*-2 chain (squares).

Figure 7a shows the average distance between equivalent carbon atoms on both chains. There is a nearly constant interchain distance of about 6 Å in the middle of the molecule, ilustrating the cylindrical shape of the DPPC molecule, an important property for the formation of stable planar bilayers by these molecules. We then investigated the relaxation of these distances (i.e., how fast they reach equilibrium) by calculating the autocorrelation function. In contrast to the actual distances there was a nearly constant increase of these relaxation times, from a few picoseconds at C1 to somewhat more than half a nanosecond for C12. This was followed, as can be seen in Figure 7a, by a marked drop at the end of the chains.

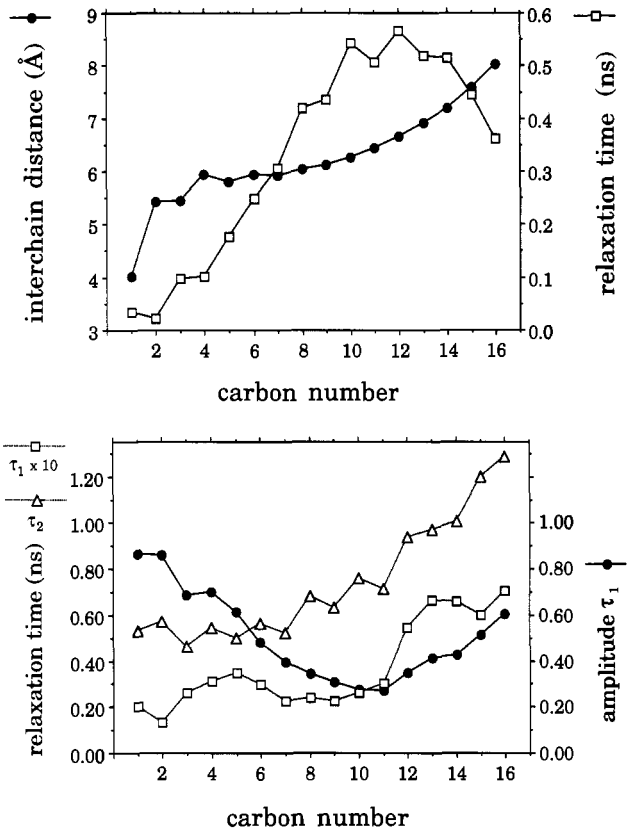

FIGURE 7: (a, Top) Average interchain distances (filled circles) and associated relaxation time (open squares) for the single-molecule simulation. Notice the nearly constant values of interchain distances in the middle of the molecule, giving the DPPC molecule its cylindrical properties, while the relaxation time estimate, based on a one-exponential fit, steadily increases. (b, Bottom) Relaxation times obtained from the two-exponential fit of the interchain distance autocorrelation functions (connected with a line). The faster component τ_1 (open squares) is multiplied by 10. The slow relaxation time τ_2 is shown with triangles. Also shown is the amplitude of the faster component (filled circles).

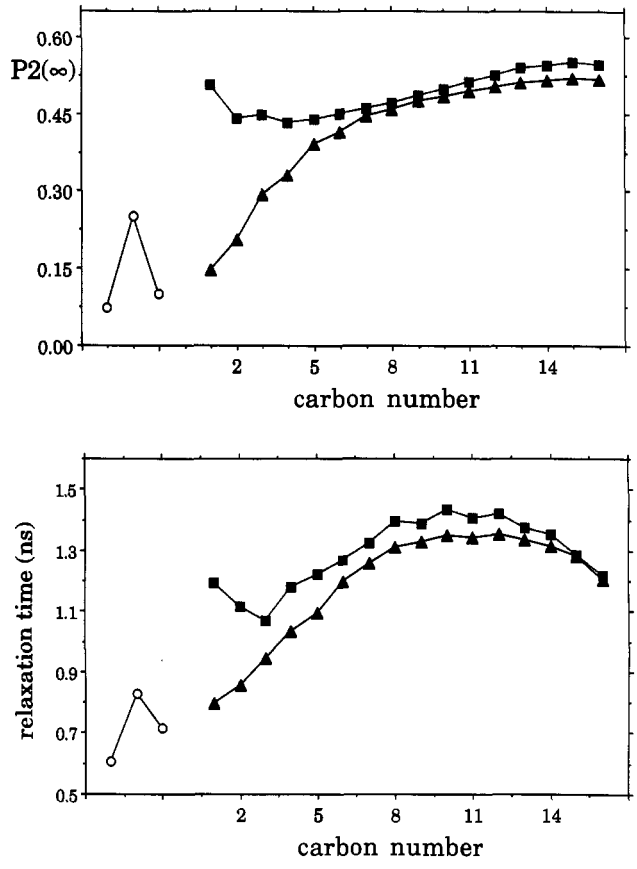

FIGURE 8: (a, Top) Limiting (or plateau) value of the P_2 autocorrelation function of the vector from the phosphorous atom to the carbon atoms in the *sn*-1 chain (filled triangles), to the *sn*-2 chain (filled squares), and to the glycerol (open circles, the carbon closest to the phosphorous is leftmost). (b, Bottom) Estimated relaxation time based on a two-exponential fit $[\sum_{i=1}^{2}(a_i\tau_i)/\sum a_i]$ for the P_2 correlation function for the vectors described in (a). Notice the presence of slow (~750 ps) relaxation of the glycerol backbone (open circles) and the very similar relaxation for the major part of the *sn*-1 chain (filled triangles) and *sn*-2 chain (filled squares).

These relaxation times, based on a one-exponential fit, are only a rough description of this process, and curve fitting with two exponentials was needed in order to extract the major features of the decay. Figure 7b shows the resulting two relaxation times together with the associated amplitude of the fast component. Except for the terminal carbon atoms, the correlation times of the rapid (τ_1) and slow (τ_2) components are relatively constant, pointing toward a common relaxation mechanism. The most likely candidates are dihedral transitions for the faster relaxation and wobbling motions of the individual chains for the slow relaxation. It is clear that as we move toward the end of the chain and as the overall relaxation time increases, the slower component becomes more important, i.e., the amplitude of τ_1 decreases. At the very end of the chain, however, dihedral transitions become more important again, in agreement with the increased torsional flexibility already discussed above. The existence of wobbling motions of the individual chains, characterized by the constant correlation time on the 500-ps time scale, seems therefore to be an important dynamic characteristic of the DPPC molecule. Because of the intramolecular nature of the interchain distances, overall rotation does not contribute to the observed relaxation.

In order to investigate global motions we calculated the P_2 correlation function for the vector from the phosphorous atom to a number of other atoms. Figure 8a shows the equilibrium $P_2(\infty)$, or the square of the associated order parameter, for the carbons in the alkane chains and the glycerol moiety, and Figure 8b shows an estimate of the relaxation time based on a two-exponential fit of the autocorrelation function decay. The order parameter is somewhat bigger at the origin of the *sn*-2 chain as compared to the *sn*-1 chain. This suggests that in our system the *sn*-1 chain is turning around the *sn*-2 chain, thereby decreasing the stress induced by the kink in the *sn*-2 chain. This was confirmed by calculating the average distance from the central *z* axis to the different carbons. For the first four carbons this distance was on average 1.69 Å larger for the *sn*-1 chain than for the *sn*-2 chain. More important is the fact that deeper into the membrane both chains have nearly identical properties, as already observed above for a number of other properties.

In contrast to the interchain distance, where only the intramolecular motions of the two chains contribute to the relaxation, it is possible that in this case additional rotational and wobbling motions of the complete molecule contribute significantly to the overall relaxation. The time scales of these wobbling motions, as estimated from a biexponential fit of the P_2 decays, are shown in Figure 8b. The curve on this figure has much the same shape as the one for the relaxation of the interchain distances (Figure 7b): an increase up to carbon 12, followed by a decrease due to the altered torsional flexibility. There are important differences, however; even at the branching of the chains we observe the presence of a slow component, and the slowest relaxation now is about 1.3 ns,

Table II: Dihedral Transitions of the Alkane Chains[a]

	$t \rightarrow g^+$	$t \rightarrow g^-$	$g^+ \rightarrow t$	$g^+ \rightarrow g^-$	$g^- \rightarrow t$	$g^- \rightarrow g^+$	g^-	t	g^+
					sn-1				
1	315	313	315	0	313	0	0.1252	0.7340	0.1409
2	206	201	206	0	201	0	0.0999	0.7981	0.1020
3	276	222	276	0	222	0	0.1136	0.7503	0.1360
4	197	217	197	0	216	0	0.1027	0.7991	0.0982
5	270	238	270	0	238	0	0.1359	0.6983	0.1658
6	206	215	204	0	215	0	0.1145	0.7958	0.0897
7	301	258	301	0	258	0	0.1262	0.7328	0.1410
8	224	229	224	0	228	0	0.1031	0.7842	0.1127
9	333	278	333	0	279	0	0.1290	0.7232	0.1478
10	271	303	271	0	303	0	0.1256	0.7521	0.1223
11	473	467	473	0	466	0	0.1291	0.7312	0.1397
12	592	586	592	0	586	0	0.1420	0.7226	0.1353
⟨⟩	305.3	293.9	305.2	0	293.8	0	0.1206	0.7518	0.1276
					sn-2				
1	67	112	67	0	112	0	0.1458	0.7664	0.0878
2	259	205	259	0	204	0	0.1472	0.7148	0.1380
3	158	221	159	0	221	0	0.1294	0.7857	0.0849
4	214	283	214	0	283	0	0.1243	0.7519	0.1238
5	182	229	182	0	229	0	0.1181	0.7882	0.0938
6	220	275	220	0	275	0	0.1574	0.7453	0.0973
7	234	238	235	0	238	0	0.1118	0.7894	0.0988
8	262	275	262	0	275	0	0.1220	0.7672	0.1108
9	274	297	274	0	298	0	0.1323	0.7558	0.1118
10	289	376	289	0	377	0	0.1426	0.7579	0.0995
11	401	473	401	0	472	0	0.1404	0.7525	0.1071
12	580	617	581	0	617	1	0.1554	0.7027	0.1419
⟨⟩	261.7	300.1	261.9	0	300.1	0.083	0.1356	0.7565	0.1080

[a] The number of transitions are given together with the fraction of trans, gauche minus (g^-), and gauche plus (g^+) states. Dihedral 1 corresponds to the torsion around the bond between C3 and C4.

nearly a nanosecond longer than for the intramolecular relaxation. The slow decay of P_2 for the glycerol carbons clearly demonstrates the presence of wobbling of this part of the molecule.

To further investigate the dynamics of the complete molecule we calculated the same correlation function for a vector from the phosphorous atom to the average position of all the carbon atoms in both chains. The $P_2(\infty)$ was 0.588, and the estimated relaxation time was 2.1 ns. (A single exponential was satisfactory in this case.) Averaging over individual chains resulted in relaxation times of 1.83 and 1.82 ns. We therefore conclude that the wobbling motions of the individual chains do not cancel each other completely at the molecular level, and that there is a significant overall wobbling of the complete molecule. This is also illustrated in Figure 9, which shows the probability distribution for the angle between the bilayer normal and the vectors described above. The averaging over the complete molecule does not result in a narrower distribution, which would be expected for independent movement of both chains. In addition, the shape of these curves shows that a cone model, characterized by an equal probability within a certain cone angle, does not fit the data. This is not completely unexpected, since the mean field is in part composed of a Maier-Saupe (1959) type potential.

Calculation of cross-correlation coefficients enabled us to further characterize the overall motions of the molecule. The angles between the bilayer normal and the vectors from the phosphorous atoms to the last five carbons in the chains all have cross-correlation coefficients between 0.429 and 0.452, clearly showing that the chains do not move independently. Even the vectors starting from the central glycerol atom to these last five carbons have cross-correlation values between 0.351 and 0.355.

The preceding analysis indicates that a very complex combination of motions, intramolecular as well as those of the complete molecule, are present. This was already apparent

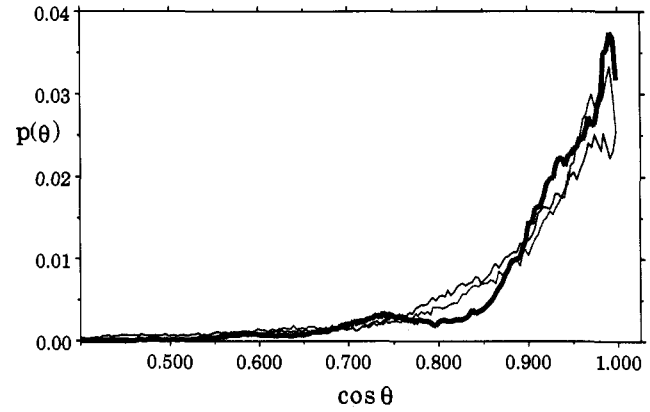

FIGURE 9: Distribution of the angle between the bilayer normal and a vector from the phosphorous atom to the average over all carbons in both chains (thick line) and over the individual chains (thin lines).

from the need for at least three or four exponentials for the T_1 calculations. It is probably not possible from a 102-ns long simulation to accurately determine the individual importance of each dihedral in this process. We expect that only much longer simulations will allow the quantitative description of these numerous individual components.

Seven-Molecule Simulations. The simulations described above made it possible to move on to the next step in our strategy, the simulation of a multimolecule system. In order to continue the study of nanosecond time scale motions, we investigated a small, seven-molecule, hexagonally packed monolayer system, containing 350 atoms (see Figure 1c). Our goal is to observe the effect of neighboring molecules, treated in atomic detail, on the equilibrium properties and the dynamics of the DPPC molecule; in other words, we want to reduce the possible bias introduced by the mean field and the Langevin dynamics approach. The model should ideally be a self-consistent one, where the boundary and central molecules

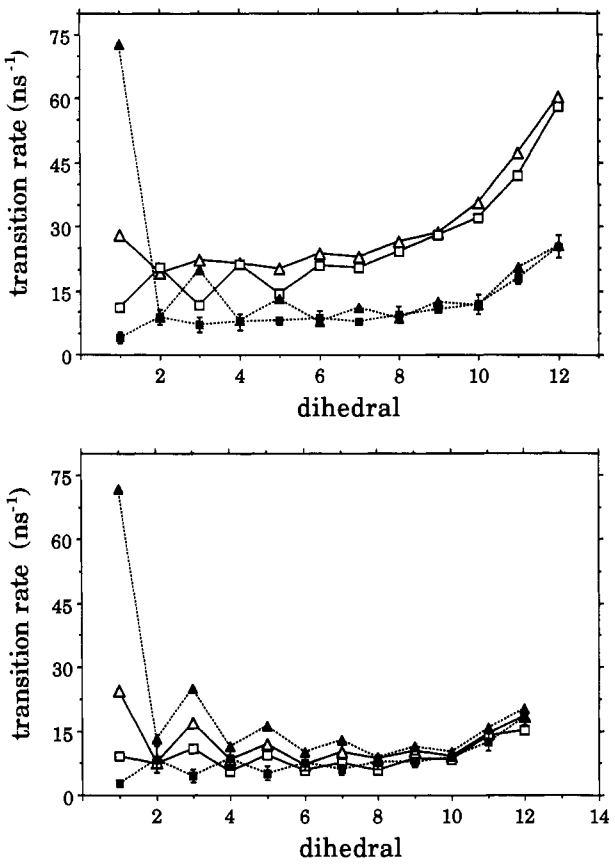

FIGURE 10: (a, Top) Dihedral transition rate (trans–gauche) of the same dihedrals described in Figure 6 for an initial 12-ns simulation with a molecular partition criterion (i.e., boundary molecules LD and central molecule MD). We compare the data of the central molecule (open symbols) versus the average of the six boundary molecules (filled symbols connected with a dotted line). Both the values for the *sn*-1 chains (triangles) and *sn*-2 chains (squares) are given. The standard deviation of the values of the boundary *sn*-2 chains is also shown. (b, Bottom) Same data as in (a), but for the 20-ns run described in the text, where the second partitioning method was used (i.e., with gradual transition between MD and LD regions).

have the same behavior, allowing the calculation of average properties of the complete system. Because intermolecular contacts become possible it is obvious that in this model changes are needed to the mean field as well as to the treatment of the dynamic effects. Below we describe the development and the preliminary results of this mean field stochastic boundary approach.

In an initial attempt, a simple molecular criterion was used for the partitioning of the system into the reaction and boundary region: the central molecule is treated with MD and the boundary molecules are treated with LD (collision frequency 25 ps^{-1}). As a marker of the dynamics of the system, the dihedral transition rates were calculated for the boundary and central molecules. Figure 10a shows the trans–gauche dihedral transition rate for the *sn*-1 and *sn*-2 chains. As already observed in the one-molecule simulation, a plateau value for the dihedrals in the middle of the chain was present, but the rates for the central molecule were much too high and outside the standard deviation of the values for the boundary molecules. A number of factors can contribute to this nonhomogeneous behavior: the lower collision frequency of the boundary atoms (25 versus 50 ps^{-1} in the one-molecule simulation), the fact that the central molecule is not always surrounded by real atoms, and inefficient energy transfer between the boundary and reaction region due to the abrupt transition from the Langevin dynamics to the molecular dynamics region. An increase of the collision frequency in the boundary to 50 ps^{-1}, however, did not improve the situation. The last reason mentioned above is most likely the predominant one, as the second partitioning method proved to be more successful (Figure 10b). In this case a gradual transition between MD and LD is obtained with a switching function, scaling the collision frequencies.

The other important parameter that needs to be changed is the strength of the mean field. In initial attempts the strength of the mean field on the boundary molecules was reduced by 50%, as compared to the single-molecule simulations described above, while no mean field forces acted on the central molecule. Although not completely unsatisfactory, this system had a major drawback. Because of the flexible nature of the alkane chains, the central molecule was sometimes no longer effectively surrounded by the boundary molecules; i.e., the chains of the central lipid protruded beyond the boundary. Such an event sometimes happened only after a few nanoseconds and resulted in deuterium NMR order parameters of the central molecule that were too low. It also prevented the system from being self-consistent.

Therefore the central molecule had to be constrained so as to mimic the effect of the phospholipids beyond the first annulus. This was achieved by applying the repulsive component of the mean field on the central molecule in a distance-dependent way: increasing the strength with increased distance from the central z axis. This improved the self-consistency of the system considerably. Subsequently some additional tuning was needed as the calculated bilayer dimension was somewhat too small and the ^{2}H NMR order parameters were too low. This was done by increasing the strength of the repulsive component on all molecules. Below we describe a 20-ns simulation where for the boundary molecules $\Phi = 0.11$ kcal/mol and $\Gamma = -10.5$ (kcal Å)/mol. For the central molecule there is no dispersive component ($\Phi = 0$ kcal/mol) and the repulsive mean field component increases, from a value of −5.5 (kcal Å)/mol at the center of the system to $\Gamma = -10.5$ (kcal Å)/mol when the distance between terminal carbon and the central z axis is more than 4 Å. Between 0 and 4 Å from the central z axis repulsive field strengths are obtained with a sigmoidal switching function and were updated every 25 steps. In parallel with the single-molecule simulation, there are probably different sets of parameters for the mean field that would yield good fits with experimental observations, but the computer time needed for equilibration prevents extensive exploration of the parameter space. (As an example we obtained very similar results for a 12-ns simulation where the repulsive component at the center of the system was −0.5 (kcal Å)/mol instead of −5.5 (kcal Å)/mol. The results of the simulation with the latter field strength are presented here as they were in slightly better agreement with experimental data.)

Figure 11 shows the deuterium NMR order parameter profile of this simulation. The standard deviations of the values for the boundary molecules were also calculated. This provides an estimate of the equilibration and it also helps in evaluating the self-consistency of the system. The objective is to obtain a central molecule with characteristics within the average standard deviation range of the boundary values. This goal is reached for the major part of the chain. Not unexpectedly, the standard deviations at the end of the chains are smaller. The characteristic plateau region, with values of about 0.2 for both chains, is again present in the model, in agreement with the experimental data (see Figure 2). The asymmetry in the interface region, caused by the kink in the *sn*-2 chain, is also present, but, due to the simple nature of the surface mimicking

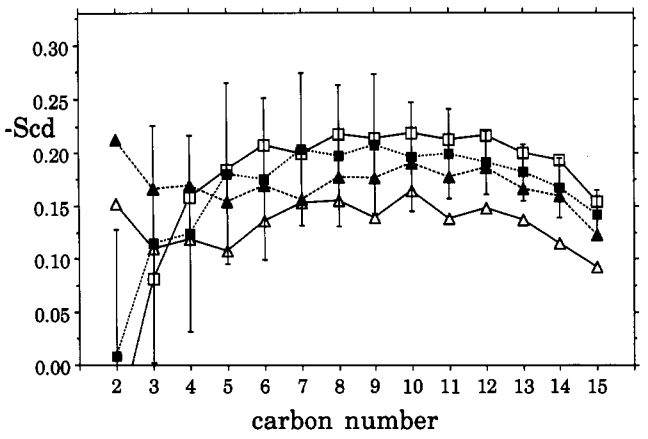

FIGURE 11: Deuterium NMR order parameters for the central molecule (open symbols) versus the average of the boundary molecules (filled symbols, dotted line). Averages over both hydrogens are given for the *sn*-1 (triangles) and *sn*-2 (squares) chains. The standard deviations for the *sn*-2 chains are indicated by error bars. Note the larger standard deviations closer to the headgroup of the molecule (due to slower relaxation). The values of the central *sn*-1 chain were also situated within this standard deviation range except for the first and last carbon, where these were situated just below this range.

the interface, the magnitude of the experimental values is not reproduced exactly (note the large standard deviations). The values for C2 on the *sn*-2 chain have most likely not converged yet within this simulation.

Figure 10b shows the dihedral transition rates for the same simulation. The improvements over Figure 10a are obvious. We already discussed the fact that the kink in the *sn*-2 chain had some effect on the dihedral transition rate at the origin of the chains during the single-molecule simulation (see Table II). This seems to be amplified in this model and results in increased frequencies for the first dihedrals in the *sn*-1 chains. The intermolecular contacts, together with the way the molecules were constrained at the interface, are the probable cause of this difference.

The average distance along the bilayer normal from the phosphorous atom to the terminal carbon atoms was 16.95 Å, close to the value obtained for the one-molecule simulation (17.9 Å). Figure 12a gives the distribution of the *z* coordinate for the terminal carbon atoms. For the central molecule this property is not expected to have completely converged during this 20-ns simulation, as was clear from Figure 4a, but its distribution is certainly very similar to that of the boundary molecules. The chains of the central molecule have been prevented from slipping through the boundary chains, a process that results in much shorter P–C16 distances. Figure 12b shows the interchain distances and further documents the self-consistency of the system and the similarity with the single-molecule simulation. The fraction of gauche conformation for all the chains in the system was 0.252, again in good agreement with experiment (Mendelsohn et al., 1989) and close to the value obtained during the single-molecule simulation.

The packing of the membrane interior was investigated by calculating the density within spheres of increasing diameters, centered at the average position of all the carbons in the chains. (This was necessary because of the highly dynamic nature of the chains.) All spheres with diameters between 3 and 10 Å had densities between 0.725 and 0.775 kg/L as compared to a density of 0.753 kg/L for pure hexadecane.

Figure 13 compares the experimentally observed field strength dependence of the T_1 relaxation times (Brown et al., 1983) with the data from the simulation. These results are

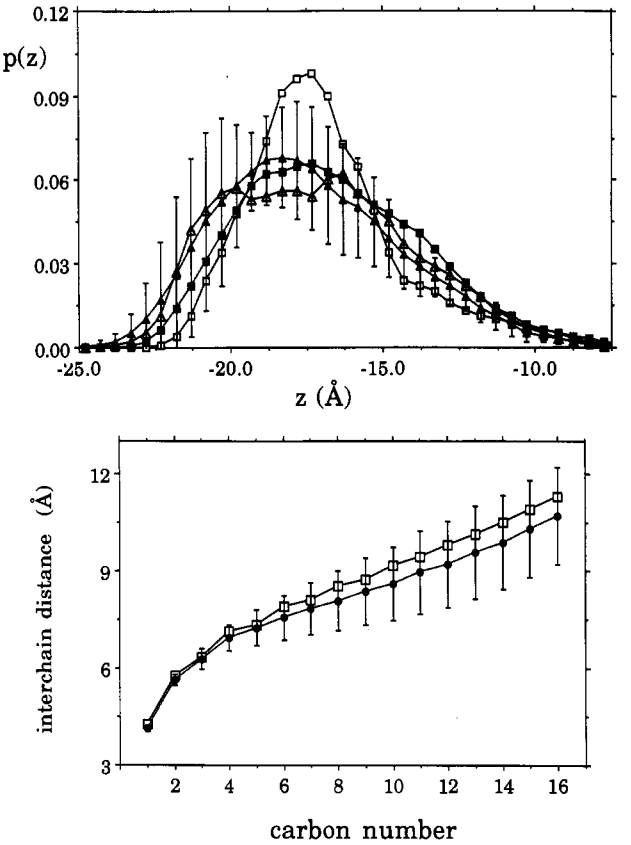

FIGURE 12: (a, Top) Probability distribution, within 0.5-Å intervals, for the *z* coordinate of the central molecule (open symbols) versus the average value of the boundary molecules (closed symbols, dotted line). (Compare with Figure 4b.) Both the *sn*-1 chain (triangles) and the *sn*-2 chain (boxes) values are shown. The standard deviation for the probabilities of the boundary *sn*-1 chains is indicated with error bars. (b, Bottom) Interchain distances of the central lipid (open squares) compared with the average and standard deviation of the boundary molecules (filled circles, dotted line). As in the single-molecule simulations, we note a plateau in the middle of the molecule. In addition, the central molecule has very much the same characteristics as the boundary molecules.

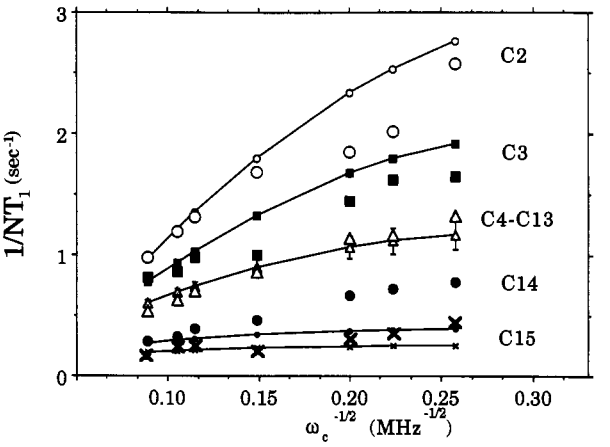

FIGURE 13: $1/NT_1$ versus $\omega_C^{-1/2}$ for the average over all *sn*-1 chains in the seven-molecule simulation compared with the experimental values obtained by Brown et al. (1983). Data from the simulations are connected with a line and have the smaller symbols: C2 (open circles), C3 (squares), C4–C13 (open triangles and standard deviation), C14 (filled circles), and C15 (x).

an averaging of the values for the seven *sn*-1 chains of the system. Also shown is the standard deviation of these values for the C4–C13 carbons. As this simulation is shorter, only the first 1500 points of the P_2 correlation function were used

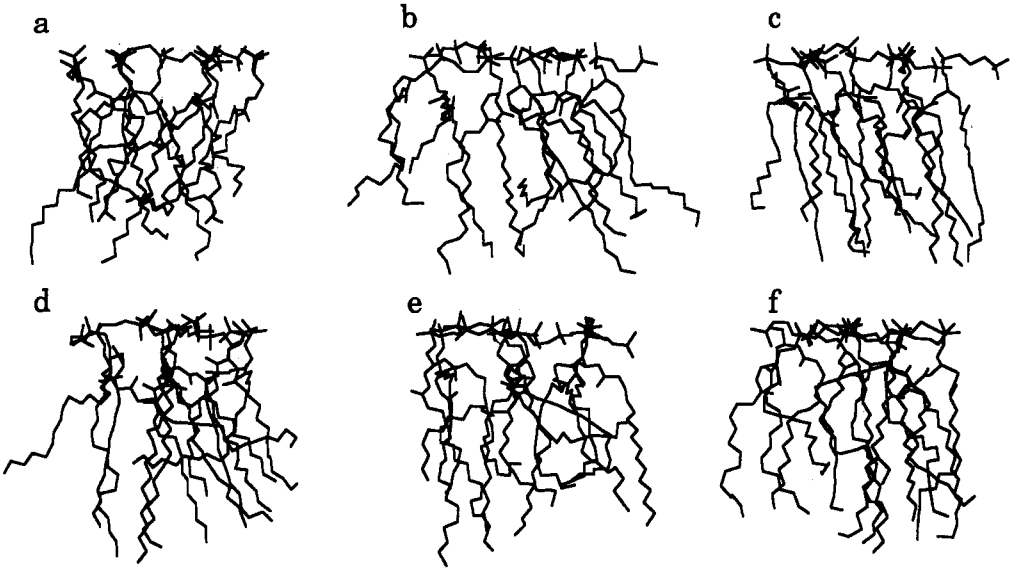

FIGURE 14: Six time frames, with 3-ns intervals, of the multimolecule simulation; a is the starting conformation.

for the calculation of T_1. Agreement between data and experiment is similar to that for the one-molecule simulation (Figure 5) and shows the presence of motions on the nanosecond time scale.

Finally, Figure 14 shows six coordinate sets at 3-ns intervals and demonstrates clearly the dynamic nature of the liquid-crystalline membrane.

Discussion

A Marcelja-type mean field allows the simulation of many of the characteristics of a DPPC molecule in a membrane environment. The average membrane dimension and deuterium NMR order profile are in good agreement with experiment. In addition, the use of Langevin dynamics enables us to simulate the dynamic effect of neighboring molecules as evidenced by the good fit with the frequency-dependent T_1 relaxation data. A more detailed analysis of the different motions of the DPPC molecule is therefore possible, as our model has atomic resolution. In this way we can expand our knowledge of the dynamics of membranes through the use of computer simulations; i.e., we obtain information that is difficult or impossible to obtain experimentally.

Analysis of the 102 000 coordinate sets from the one-molecule simulation showed a number of interesting features of the DPPC molecule, some of which are in close agreement with the single-chain simulations reported by Pastor et al. (1988a,b). As demonstrated in Figures 3 and 4, the volume spanned by one molecule, or its allowed conformational space, is clearly very large, and therefore relatively long simulations are necessary in order to obtain reliable estimates of certain equilibrium properties. Dynamically, we note the importance of the constant transition frequency in the middle of the chain and the increased torsional flexibility at the end of the molecule. This results in the liquidlike characteristics of the membrane interior and contributes to the constant order in the middle of the DPPC molecule. The other important dynamic aspect of the phospholipid is the motions occurring on the nanosecond time scale. While previously, in order to obtain agreement with the experimental data, these motions had to be added in an analytical, model-dependent way (Pastor et al., 1988b), it was possible to observe them directly in this study. In agreement with the model proposed by Rommel et al. (1988) there is wobble of the complete molecule in addition to the presence of motions of the individual chains on the nanosecond time scale. This was deduced by analyzing the interchain distance relaxation, a intramolecular property that is not dependent on overall motions of the complete DPPC molecule.

The different dynamic characteristics of the membrane phospholipid molecule are clearly illustrated in Figure 3. On the 100-fs time scale (Figure 3a) only vibration within the gauche and trans wells is observed. The 1-ps time scale is not significantly different, with the exception of an isolated dihedral transition at the end of the chains, where the transition rates are significantly higher. By 10-ps (Figure 3c), transitions have occurred at different positions along the chain. As we move into the 100-ps (Figure 3d) time scale, multiple tran-

Table III

Bond Potential: $E_b = \sum k_b(r - r_0)^2$		
bond	r_0	k_θ [kcal/(mol Å^n)]
CH_2—CH_2	1.530	260
CH_2—CH_3	1.530	260
CH_2—CH	1.526	260
CH_2—C	1.522	317
—O—C	1.330	580
—O—CH_2	1.425	320
—O—P	1.610	230
=O—C	1.229	570
—O—P	1.480	525
N—CH_2	1.471	367
Bond Angle Potential: $E_\theta = \sum k_\theta(\theta - \theta_0)^2$		
angle	θ_0 (deg)	k_θ [kcal/(mol rad^2)]
CH_2—CH_2—CH_2	45	109.28
CH_2—CH_2—CH_3	45	109.28
CH_2—CH_2—C	63	112.4
CH_2—CH_2—O—	80	109.5
CH_2—CH_2—N	80	111.2
CH_2—CH—CH_2	45	109.28
CH_2—CH—O—	80	109.5
CH_2—C—O—	85	114
CH_2—C=O	80	120.4
CH_2—O—C	100	111.8
CH_2—O—P	100	120.5
CH_2—N—CH_3	60	109.5
CH_3—N—CH_3	60	109.5
CH—CH_2—O—	80	109.5
CH—O—C	100	111.8
—O—C=O	80	120.4
—O—P—O—	45	102.6
—O—P—O	100	108.23
—O—P—O	140	119.9

Table IV[a]

Torsion Angle Potential: $E_\phi = \sum k[1 + \cos(n\phi - \gamma)]$			
torsion	n	γ (rad)	k (kcal/mol)
CH_2—CH_2—CH_2—C	3	0	1.4
CH_2—CH_2—C—O—	6	0	0.1
CH_2—CH_2—N—CH_3	3	0	0.47
CH_2—CH—CH_2—O—	−3	0	1.4
	2	0	0.1
CH_2—CH—O—C	−3	0	0.72
	2	0	0.1
CH_2—C—O—CH_2	−2	3.142	10
	1	0	0.65
CH_2—C—O—CH	−2	3.142	10
	1	0	0.65
CH_2—O—P—O	3	0	0.25
CH_2—O—P—O—	−3	0	0.25
	2	0	0.75
CH_2—CH_2—O—P	3	0	1.45
CH—CH_2—O—P	3	0	1.45
C—O—CH_2—CH	−3	0	1.45
	2	0	0.1
—O—CH_2—CH—O—	−3	0	1
	2	0	0.5
—O—CH_2—CH_2—N	3	0	1.4

[a] Improper torsion potential, $E_\omega = \sum k_\omega(\omega - \omega_0)^2$; planarity of the carbonyl bond; chirality of the central glycerol carbon; $k_b = 40$ [kcal/(mol rad^2)]. For the dihedral angles of the alkane chains, C-H_2—CH_2—CH_2—CH_2 and CH_2—CH_2—CH_2—CH_3, we use the Ryckaert-Bellemans potential (1975): $E_\phi = \sum\sum_{k=0}^{5} C_k(\cos\phi)^k$; $C_0 = 2.2177$, $C_1 = 2.9052$, $C_2 = -3.1358$, $C_3 = -0.731\,28$, $C_4 = 6.2715$, and $C_5 = 7.5274$ kcal/mol.

sitions have taken place between each time frame, and the presence of some rotation of the molecule is apparent. It is only at the 1-ns time scale (Figure 3e) that a significant amount of wobble of the complete molecule is present, as best illustrated by the glycerol backbone. Figure 3f, nearly spanning the complete simulation, does not yield a very different picture when compared to Figure 3e, in agreement with the maximum relaxation times of 1–2 ns obtained directly from the trajectories. We point out, however, that the reliable determination of these dynamic features is not possible unless the trajectories are several times longer than the slowest relaxation time (Zwanzig & Ailawadi, 1969); in other words, only when similar figures, such as parts e and f of Figure 3 can be juxtaposed can valid conclusions be made about the dynamics of the system.

A more detailed analysis showed the very complex nature and interdependence of all these motions. It is therefore clear that a model without atomic resolution and not including every degree of freedom cannot accurately describe all the observed motions. A large number of dihedral angles plays a role in both intramolecular relaxation as well as the overall motions of the complete molecule. The quantitative determination of the impact of each of these dihedrals in the dynamics of the complete molecule can only be determined from much longer simulations. The calculation of cross-correlation coefficients also showed that the two chains do not behave completely independently, thereby making the system even more complex. These cross-correlations also emphasize the need for multimolecule simulations, because such effects most probably also exist between neighboring molecules and may affect the equilibrium and dynamic properties of DPPC in a different way as compared to the mean field in the single-molecule simulation.

We initiated such simulations with a small number of phospholipid molecules. Our system contains 350 atoms and remains small enough to allow the calculation of the multinanosecond trajectories that are needed to adequately sample conformational space. We used a stochastic boundary molecular dynamics approach where conventional MD is used on those atoms that are surrounded by other explicitly treated atoms and where atoms in the boundary layer are treated with Langevin dynamics plus a mean field, to mimic volume exclusion and collision effects from molecules not included in the system. The necessary changes to the mean field and the method for partitioning the system into a Langevin and molecular dynamics regions were investigated, and some factors that contribute to the self-consistency of the system were determined. The preliminary data we presented here clearly show the feasibility of this approach.

During the development of the model, the importance of a gradual transition between the molecular dynamics and Langevin dynamics region became apparent (Figure 10).

Table V: The Nonbonded Potential

$$E_{vdW} = \sum_{excl(i,j)} \left(\frac{A_{ij}}{r_{ij}^{12}} - \frac{B_{ij}}{r_{ij}^{6}} \right)$$

	C	CH	CH_2	CH_3	N	=O	—O—	—O	P
				A [(kcal Å^{12})/mol × 10^{-6}]					
C	0.7899								
CH	0.6841	0.5925							
CH_2	1.6024	0.8704	3.0796						
CH_3	1.9321	1.2323	3.7123	4.4720					
N	0.6450	0.5586	0.8206	1.1618	0.5266				
=O	0.4405	0.3815	0.5702	0.8207	0.3597	0.2306			
—O—	0.4534	0.3926	0.5847	0.8387	0.3702	0.2405	0.2502		
—O	0.4405	0.3815	0.5702	0.8207	0.3597	0.2306	0.2405	0.2306	
P	2.2350	1.9355	2.8009	3.9081	1.8248	1.3166	1.3395	1.3166	6.0259
				B [(kcal Å^6)/mol]					
C	615.79								
CH	533.27	461.83							
CH_2	800.56	601.50	1125.3						
CH_3	965.30	756.75	1356.5	1634.1					
N	5027.6	435.41	567.09	713.48	410.50				
=O	522.45	452.47	594.43	754.07	426.59	429.48			
—O—	493.27	427.18	560.19	709.39	402.72	408.20	387.42		
—O	522.45	452.47	594.43	754.07	426.59	429.48	408.20	429.48	
P	1176.9	1019.2	1317.4	1645.5	960.87	1026.3	963.34	1026.3	2195.6

Because of the large degree of freedom of the phospholipid molecule, it was possible that during the simulation the central molecule protruded beyond the boundary where it was no longer surrounded by other molecules. Therefore a small mean field potential was needed on the central molecule, mimicking, in a crude way, the interactions with the phospholipid molecules beyond the immediate six neighbors. The simulation of a larger system, with an additional layer of phospholipids, will thus ultimately be needed for a completely mean field free reaction zone.

After some tuning of the mean field parameters, we obtained a dynamic membrane model that was in good agreement with the available experimental data. The equilibrium and dynamic properties of the central chain were not significantly different from those at the boundary, demonstrating the possibilities of a stochastic boundary approach for the efficient simulation of a liquid-crystalline system. In addition, the results of the central molecule in the multimolecule assembly were very similar to those obtained in the single-molecule simulation, and this further validates the use of a mean field in the single-molecule simulation.

A look at Figure 14, where different time frames, at 3-ns intervals, are shown, clearly illustrates the dynamic nature of the liquid-crystalline phospholipid membrane. It is obvious that the disorder is much bigger than what most textbook pictures of membranes might suggest. In addition we would like to recommend using phospholipid conformations sampled from these trajectories for more realistic computer graphics representations of membrane systems such as membrane proteins in their lipid environment.

We think this methodology will be very useful in future studies of the dynamics of membranes. It should also help in the interpretation of some experimental results. Due to the general properties of the molecular mechanics model it will be possible, by replacing the central molecule, to extend this methodology to the study of the interaction of small molecules (and ultimately proteins) with membranes and phospholipid monolayers. Most important, however, is that, in contrast to the experimental observations, a very detailed picture of the equilibrium and dynamic properties of lipid molecules in a membrane is obtained from these computer simulations.

ACKNOWLEDGMENTS

We thank Dr. M. Carson and the UAB Center for Macromolecular Crystallography for generous amounts of computer time. Special thanks to Dr. Robert Tan for the *yammp* source code as well as for assistance and invaluable advice in programming and use of the computers.

APPENDIX: MOLECULAR MECHANICS PARAMETERS

The total energy of the system, or the potential energy function, consists of several terms. It is a standard energy function used for the modeling of proteins or nucleic acids (McCammon & Harvey, 1987; Weiner et al., 1984), with the addition of terms for the mean field ($E_{rep} + E_{disp}$) (Tables III–V):

$$E_{tot} = E_b + E_\theta + E_\omega + E_\phi + E_{vdW} + E_{constr} + E_{sur} + E_{rep} + E_{disp}$$

Registry No. DPPC, 2644-64-6.

REFERENCES

Berkowitz, M., & McCammon, J. A. (1982) *Chem. Phys. Lett. 90*, 215–217.

Brooks, C. L., Brunger, A., & Karplus, M. (1985) *Biopolymers 24*, 843–865.

Brown, M. F., Ribeiro, A. A., & Williams, G. D. (1983) *Proc. Natl. Acad. Sci. U.S.A. 80*, 4325–4329.

Brunger, A., Brooks, C. B., & Karplus, M. (1984) *Chem. Phys. Lett. 105*, 495–498.

Cevc, G., & Marsh, D. (1987) *Phospholipid Bilayers*, John Wiley & Sons, New York.

Edholm, O., & Johansson, J. (1987) *Eur. Biophys. J. 14*, 203–209.

Egberts, E. (1988) Molecular Dynamics Simulation of Multibilayer Membranes, Ph.D. Thesis, Rijksuniversiteit, Groningen.

Egberts, E., & Berendsen, H. J. C. (1988) *J. Chem. Phys. 89*, 3718–3726.

Elder, M., Hitchcock, P., Mason, R., & Shipley, G. G. (1977) *Proc. R. Soc. London A 354*, 157–170.

Gennis, R. B. (1989) *Biomembranes. Molecular Structure and Function*, Springer Verlag, New York.

Gruen, D. W. R. (1985) *J. Chem. Phys. 89*, 146–153.

Harris, J., & Rice, S. A. (1988) *J. Chem. Phys. 89*, 5898–5908.

Helfand, E. (1978) *J. Chem. Phys. 69*, 1010–1018.

Helfand, E. (1984) *Science 226*, 647–650.

Jain, M. (1988) *Introduction to Biological Membranes*, John Wiley & Sons, New York.

Lewis, B. A., & Engleman, D. M. (1983) *J. Mol. Biol. 166*, 211–217.

Lipari, G., & Szabo, A. (1982) *J. Am. Chem. Soc. 104*, 4546–4559.

Maier, W., & Saupe, A. (1959) *Z. Naturforsch., A 14*, 882–889.

Marcelja, S. (1973) *Nature 241*, 451–452.

Marcelja, S. (1974) *Biochim. Biophys. Acta 367*, 165–176.

McCammon, J. A. & Harvey, S. C. (1987) *Dynamics of Proteins and Nucleic Acids*, Cambridge University Press.

Mendelsohn, R., Davies, M. A., Brauner, J. W., Schuster, H. F., & Dluhy, R. A. (1989) *Biochemistry 28*, 8934–8939.

Northrup, S. H. (1984) *J. Phys. Chem. 88*, 3441–3446.

Northrup, S. H., & Cuvin, M. S. (1985) *J. Phys. Chem. 89*, 4707–4713.

Pastor, R. W. (1990a) in *Molecular Description of Biological Membrane Components by Computer Aided Conformational Analysis* (Brasseur, R., Ed.) Vol. I, pp 171–201, CRC Press.

Pastor, R. W., & Karplus, M. (1989) *J. Chem. Phys. 91*, 211–218.

Pastor, R. W., Venable, R. M., & Karplus, M. (1988a) *J. Chem. Phys. 89*, 1112–1227.

Pastor, R. W., Venable, R. M., Karplus, M., & Szabo, A. (1988b) *J. Chem. Phys. 89*, 1128–1140.

Pastor, R. W., Brooks, B. R., & Szabo, A. (1988c) *Mol. Phys. 65*, 1409–1419.

Pastor, R. W., Venable, R. M., & Karplus, M. (1990b) *Proc. Natl. Acad. Sci. U.S.A.* (in press).

Press, W. H., Flannery, B. P., Teukolsky, S. A., & Vetterling, W. T. R. (1988) *Numerical Recipes in C. The Art of Scientific Computing*, Cambridge University Press, Cambridge.

Rommel, E., Noack, F., Meier, P., & Kothe, G. (1988) *J. Phys. Chem. 92*, 2981–2987.

Ryckaert, J. P., & Bellemans, A. (1975) *Chem. Phys. Lett. 30*, 123–125.

Schindler, H., & Seelig, J. (1975) *Biochemistry 14*, 2283–2287.

Seelig, A., & Seelig, J. (1974) *Biochemistry 23*, 4839–4845.

Seelig, J., & Seelig, A. (1980) *Q. Rev. Biophys. 13*, 19–61.

Tan, R. K. Z., & Harvey, S. C. (1989) *J. Mol. Biol. 205*, 573–592.
van der Ploeg, P., & Berendsen, H. J. C. (1982) *J. Chem. Phys. 76*, 3271–3276.
van der Ploeg, P., & Berendsen, H. J. C. (1983) *Mol. Phys. 49*, 233–248.
Verlet, L. (1967) *Phys. Rev. 159*, 98.
Watanabe, K., Ferrario, M., & Klein, M. (1988) *J. Phys. Chem. 92*, 818–821.
Weiner, S. J., Kollman, P. A., Case, D. A., Singh, U. C., Ghio, C., Alagona, G., Profeta, S., & Weiner, P. (1984) *J. Am. Chem. Soc. 106*, 765–784.
Wendoloski, I. J., Kimatian, S. J., Schutt, C. E., & Salemme, F. R. (1989) *Science 243*, 637–638.
Zaccai, G., Buldt, G., Seelig, A., & Seelig, J. (1979) *J. Mol. Biol. 134*, 693–706.
Zwanzig, R., & Ailawadi, N. K. (1969) *Phys. Rev. 182*, 280–284.

Frequency-Domain Fluorescence Spectroscopy Resolves the Location of Maleimide-Directed Spectroscopic Probes within the Tertiary Structure of the Ca-ATPase of Sarcoplasmic Reticulum†

Diana J. Bigelow* and Giuseppe Inesi
Department of Biological Chemistry, University of Maryland School of Medicine, 660 West Redwood Street, Baltimore, Maryland 21201

Received July 17, 1990; Revised Manuscript Received November 14, 1990

ABSTRACT: We have used fluorescence spectroscopy to characterize three covalently bound spectroscopic maleimide derivatives with respect to their location within the tertiary structure of the Ca-ATPase of sarcoplasmic reticulum (SR). These derivatives include (1) 2-(4′-maleimidoanilino)naphthalene-6-sulfonic acid, (2) 4-(dimethylamino)azobenzene-4′-maleimide, and (3) fluorescein 5′-maleimide. Biochemical assays demonstrate that modification with any of these three derivatives results in the same functional effects, observed following derivatization of cysteines 344 and 364 by *N*-ethylmaleimide [Saito-Nakatsuka et al. (1987) *J. Biochem. (Tokyo) 101*, 365–376]. These residues bracket the ATPase's phosphorylation site (Asp 351) and thus may provide spectroscopic probes of the protein's conformation in this essential region. In agreement with sequencing results, SDS–polyacrylamide gels show that maleimide-modified SR exhibits fluorescence exclusively on the A_1 tryptic fragment of the Ca-ATPase. Extensive tryptic digestion followed by centrifugation demonstrates essentially all of the fluorescence was associated with the soluble rather than insoluble (membrane-associated) peptides, confirming the predicted extramembraneous location of these residues. Utilizing frequency-domain fluorescence spectroscopy, we were able to recover the transient effects associated with a distribution of donor–acceptor distances. We find from these fluorescence resonance energy transfer measurements that covalently bound maleimide probes are 36 Å apart, independent of whether a discrete distance is assumed or a distance distribution model is utilized, in which the conformational variability of the protein is taken into account. While a unimodal distance distribution is adequate to describe the intensity decay associated with maleimide-directed donor–acceptor pairs, a bimodal distribution of distances is necessary to describe the frequency response associated with the energy transfer between maleimide-directed chromophores and other covalently bound probes on the Ca-ATPase, consistent with the large spatial separation observed between maleimides. We recover mean distances of 42 and 77 Å between maleimide sites and bound FITC (Lys 515) and mean distances of 28 and 37 Å between the maleimide- and the iodoacetamide-directed probes (Cys 670 and 674, whose close proximity approximates a single locus). The measured distances are presented in a model and have permitted us to describe a unique arrangement of these covalently bound probes within both the secondary and tertiary structure of the Ca-ATPase. The resolution inherent in the frequency-domain fluorescence technique to multiple donor–acceptor distances should be generally applicable to a wide range of biological systems in which specific labeling of single unique donor–acceptor sites is not feasible.

Reactive cysteines of the Ca-ATPase of sarcoplasmic reticulum (SR)[1] have often been effectively utilized as convenient sites of attachment for spectroscopic probes, allowing the elucidation of many of the protein's structural features and conformational changes (Champeil et al., 1976; Coan & Inesi, 1977; Hidalgo et al., 1978; Thomas & Hidalgo, 1978; Coan et al., 1979; Guillain et al., 1981; Miki et al., 1981; Yasuoka-Yabe & Kawakita, 1983; Bigelow et al., 1984; Bigelow & Thomas, 1987; Squier et al., 1988). Iodoacetamide and maleimide derivatives have frequently been used due to the dif-

† Supported by NHBLI (PO1 HL27867).
* To whom correspondence should be addressed at the Department of Biochemistry, The University of Kansas, Haworth Hall, Lawrence, KS 66045-2106.

[1] Abbreviations: SR, sarcoplasmic reticulum; NEM, *N*-ethylmaleimide; ANSmal, 2-(4′-maleimidoanilino)naphthalene-6-sulfonic acid; DABmal, 4-(dimethylamino)azobenzene-4′-maleimide; Fmal, fluorescein 5′-maleimide; FITC, fluorescein 5′-isothiocyanate; IAEDANS, 5-[[2-[(iodoacetyl)amino]ethyl]amino]naphthalene-1-sulfonic acid; IAF, 5-(iodoacetamido)fluorescein.

0006-2960/91/0430-2113$02.50/0